Quantitative Study for Oxygen Reduction and Evolution in Aprotic Organic Electrolytes at Gas Diffusion Electrodes by DEMS

C. J. Bondue,[a] A. A. Abd-El-Latif,[a,b] P. Hegemann,[a] and H. Baltruschat[a,*,z]

[a]*Institut für Physikalische und Theoretische Chemie, Universität Bonn, D-53117 Bonn, Germany*
[b]*National Research Centre, Physical Chemistry Department, 12311 Cairo, Egypt*

Cyclic voltammetry and differential electrochemical mass spectrometry (DEMS) have been combined to study the cycling performance of the oxygen reduction reaction (ORR) and the oxygen evolution reaction (OER) at a gold electrode in non-aqueous dimethyl sulfoxide (DMSO) and *N*-methyl-2-pyrrolidone (NMP) based $LiClO_4$ and $N(Bu)_4ClO_4$ containing electrolytes. An Au-sputtered Teflon membrane (with a thickness of Au of only 50 nm resulting in an extremely short pore length on the electrolyte side) has been used as a model for a gas diffusion electrode (GDE) in this study: The oxygen molecules diffuse through a membrane from the gas side and are reduced at Au on the electrolyte side. The redox couple $O_2^{-\bullet}/O_2$ is the predominant reaction during ORR in $N(Bu)_4ClO_4$ based electrolytes whereas the calculated number of electron transferred is one. In presence of Li-ions, the average number of electrons transferred is 2 during oxygen reduction, which indicates the formation and oxidation of peroxide during ORR and OER respectively. The mass spectrometric cyclic voltammograms (MSCVs) data show that the maximum true coulombic efficiency of OER/ORR in DMSO and NMP is about 60% and 25%, respectively, with the evolution of CO_2 in NMP at 0.1 V (vs. Ag^+/Ag) due to the decomposition of the electrolyte.
 [DOI: 10.1149/2.0871503jes]

Manuscript submitted September 18, 2014; revised manuscript received December 30, 2014. Published January 9, 2015.

One of today's challenges is the development of an energy storage system that can provide both high capacity and good cycling performance. Secondary lithium-air batteries are promising candidates as they provide a high theoretical capacity. However in practice, cycling performance is bad. The key step in discharging these batteries is the reduction of oxygen present in air. So far the oxygen reduction reaction has been investigated thoroughly in aqueous media, but only little fundamental research has been done in non-aqueous solvents.

The first non-aqueous lithium-air battery was introduced in 1996 by Abraham and Jiang[1] as an alternative energy storage system for future applications. The specific energy of a Li-air battery amounts to 5.21 kWh/kg (including the weight of O_2), based on the assumption that Li fully reacts with O_2 to form Li_2O.[1] However, in practice the route to Li_2O has proven irreversible. Hence, a more reasonable specific energy of 3.5 kWh/kg is obtained assuming lithium peroxide (Li_2O_2)[2] as the sole discharge product. In practice Li-air batteries suffer from rapid capacity fading due to several obstacles such as poisoning the lithium electrode with CO_2,[3] moisture and the instability of organic electrolyte used today against superoxide ion radical ($O_2^{-\bullet}$).[4] One main challenge to overcome in the attempt to develop a reversible Li-O_2 batteries with high capacity is the selection of an appropriate non-aqueous electrolyte which is characterized by high stability in the presence of lithium oxide species and a wide potential window. There are further requirements for the electrolyte in battery applications, such as low flammability, low vapor pressure and a large temperature range in which it is present in liquid form.

Li-air batteries based on the non-aqueous organic carbonate electrolyte showed poor cycling efficiency due to the decomposition of the electrolyte to lithium carbonate ($LiCO_3$) and lithium alkylcarbonate (RO-(C=O)-OLi)[5,6] that accumulated on the cathode. In addition dendrite formation was observed.[7]

Read[8] reported an excellent rate capability and good stability of ether-based electrolyte in Li/O_2 cell. Recently, Scrosati[9] showed by XRD that tetraglyme-$LiCF_3SO_3$ is a convenient electrolyte for Li-air batteries whereas Bruce[10] using XRD, FTIR- and NMR techniques demonstrated that tetraglyme-$LiPF_6$ is not a suitable electrolyte as it decomposes in the first few cycles to form a mixture of Li_2CO_3, HCO_2Li, CH_3CO_2Li, polyethers/esters, CO_2, and H_2O.[10] Also Laoire et al. attributed the low rechargeability of the uncatalyzed Li-O_2 battery using tetraglyme-$LiPF_6$ based electrolyte to the poor cycling efficiency of the Li anode and to the high impedance associated with the deposition of Li_2O_2 on the cathode.[11]

Recently, dimethyl sulfoxide (DMSO)[12,13] and *N*-methyl-2-pyrrodione (NMP)[14,15] have been suggested as candidates for a rechargeable non-aqueous Li-air battery because they show high stability versus the superoxide ion and the main discharge product is Li_2O_2.

In general it seems to be established in literature that the oxygen reduction in organic electrolytes containing lithium ions results in the formation of lithium peroxide.[12,16–18] For that a number of techniques have been employed ranging from purely kinetic considerations after recording a CV to more meaningful techniques such as XRD-profiling,[16] SEM-imaging[18] and FTIR-,[12] Raman-[12] and XP-spectroscopy[17] of the discharge electrode.

Employing cyclic voltammetry (CV) and rotating disk electrode (RDE) techniques, Abraham group[13,16] concluded that DMSO is a practical electrolyte for Li-O_2 batteries since it facilitates the reversibility of oxygen reduction/oxidation reaction. On the other hand, Li_2O_2 has been reported as the major discharge product at a nanoporous gold electrode[12] or at a TiC-based cathode[19] using 0.1 M $LiClO_4$ in DMSO as the electrolyte in Swagelok design cell for DEMS; the number of electrons per O_2 molecule during discharging or charging is 2.

NMP is one of the most stable organic solvents versus the superoxide anion radical. It has a higher theoretical energy barrier (>40 kcal/mol) than that of organic carbonates (≈20 kcal/mol) for the nucleophilic attack at any ring carbon atom during oxygen reduction reaction.[15]

Differential electrochemical mass spectrometry (DEMS) has become a versatile tool for the on-line detection of volatile products and intermediates which are formed during the electrochemical reaction either in aqueous or non-aqueous electrolytes.[20] So far, for instance, reductive and oxidative decomposition products of organic carbonate electrolyte solutions used in Li-ion batteries were detected by DEMS using a porous working electrode[21–23] or headspace cell.[24–27] Using a headspace cell for DEMS, oxygen evolution from a Li-O_2 battery featuring a $LiPF_6$/PC electrolyte was detected.[28]

In the papers mentioned thus far only the apparent coulombic efficiency of ORR and OER was determined by comparing the faradaic

*Electrochemical Society Active Member.
[z]E-mail: baltruschat@uni-bonn.de

charge transferred during discharge (Q_c) with that transferred upon charging (Q_a). Based on the faradaic charges, Laoire et al.[11] for instance found that the Q_a/Q_c is 95% in TEGDME-$LiPF_6$ based electrolyte whereas Wang et al.[14] reported the high ratio (97%) in NMP-$LiClO_4$ based electrolyte. Since the apparent coulombic efficiency is not a sufficient criterion for the real cycleability of Li-O_2 batteries, McCloskey et al.[29] determined the true coulombic efficiency (the ratio of evolved and reduced amounts of oxygen) of Li-O_2 battery for a variety of organic solvents in a head space cell combined with DEMS. With this setup the true coulombic efficiency of a Li-O_2 battery with a DMSO-TFSI and NMP-TFSI based electrolyte was found to be 50 and 60%, respectively.[29] The term "coulombic efficiency," typically used in batteries research for the ratio of charge during charging and discharging has to be well distinguished from the current efficiency, relating the true amount of formed or consumed species to the amounts as calculated from Faraday's law. A quantitative study, done by McCloskey et al.[30] (again using a head space DEMS cell), demonstrated that the charging and discharging peaks in a DME-LiTFSI based electrolyte are due to oxygen reduction and oxidation reactions with $2e^-/O_2$ without any evidence for LiO_2 or Li_2O formation at any potential. However only 60% of oxygen reduced are re-evolved in this experiment. Using the same cell set-up, Barile and Gewirth[31] reported that the presence of Au nanoparticles as a cathode improve the cycleability of the cell and increase the amount of evolved oxygen gas during the charge process. On the other hand, the presence of Pt, Pd or Cu(II)O reduces the cell performance.

DEMS combined with a sealed battery designed cell was applied for quantitative gas evolution analysis during charging of Li-O_2 battery in propylene carbonate (PC) and diglyme-LiTFSI based electrolytes.[32] The dominant product is O_2 in case of diglyme electrolyte whereas PC is not stable at high potential producing CO_2 gas.

In some of the experiments described here, we mimic the applied air breathing battery by supplying oxygen from atmosphere at a gas diffusion electrode. In this study a porous working electrode (50 nm Au sputtered onto a teflon membrane) serves as a model for gas diffusion electrodes. The apparent coulombic efficiency was calculated from the faradaic charge obtained from cyclic voltammetry. However the true coulombic efficiency of oxygen evolution/consumption in NMP-$LiClO_4$ and DMSO-$LiClO_4$ based electrolytes were determined from the corresponding ionic charge obtained by means of DEMS using a conventional DEMS cell. In the later case oxygen was supplied to the electrode from solution. The main difference (and advantage for fundamental research) is that the electrode is relatively smooth (as compared to battery electrodes which have been used in the past for similar measurements) with a roughness factor of about 10 and a pore length on the electrolyte site of only about 50 nm. Therefore there are no diffusion effects in the pores and no complications, i.e. due to pore clogging (a severe problem observed in model batteries), are to be expected. This enables us to investigate the underlying electrochemistry and its limitations to the concept of lithium-air batteries.

Experimental

Mass spectrometry combined with the conventional DEMS cell was used in this study to detect in situ the volatile products and intermediates which are produced during electrochemical reactions.[20,33]

The DEMS cell setup is schematically shown in Figure 1. The working electrode and a 6 mm i.d-Teflon spacer are clamped between the glass body and the steel holder whereas the porous steel frit works as a mechanical support for the Au-sputtered Teflon membrane working electrode.

This cell is directly connected to the vacuum system through an angle valve and a T-piece. This cell also has the advantage of the small electrolyte volume needed ($\leq$ 1.5 ml) for an experiment.

The gold-sputtered (50 nm Au) Teflon membrane serves both as a working electrode and as the electrolyte-vacuum interface. Due to the high surface tension of the electrolyte used here, they do not penetrate the capillaries of the membrane. An Au wire was used as a counter electrode. As a reference electrode a silver wire immersed in a solution of 0.1 M $AgNO_3$ in the solvent used to prepare the working electrolyte was employed. Electrically the reference electrode was connected to the working electrode compartment by a salt bridge made from a Teflon tube filled with the $AgNO_3$ solution. In order to protect the working electrolyte from contamination with silver ions the Teflon tube was closed with a rough glass bead. Ion migration along the glass surface maintains sufficient conductivity. A drawing of the reference electrode is shown in Figure 2.

The standard electrode potentials of the Ag^+/Ag and the Li^+/Li couple were determined versus the standard hydrogen electrode (SHE) in several non-aqueous solvents by Gritzner.[34] Taking these values into account the reference electrode's potential is calculated to be +0.43 V in DMSO and +0.54 V in NMP versus SHE. Versus the Li^+/Li couple the respective potentials are −3.89 V and −3.80 V.

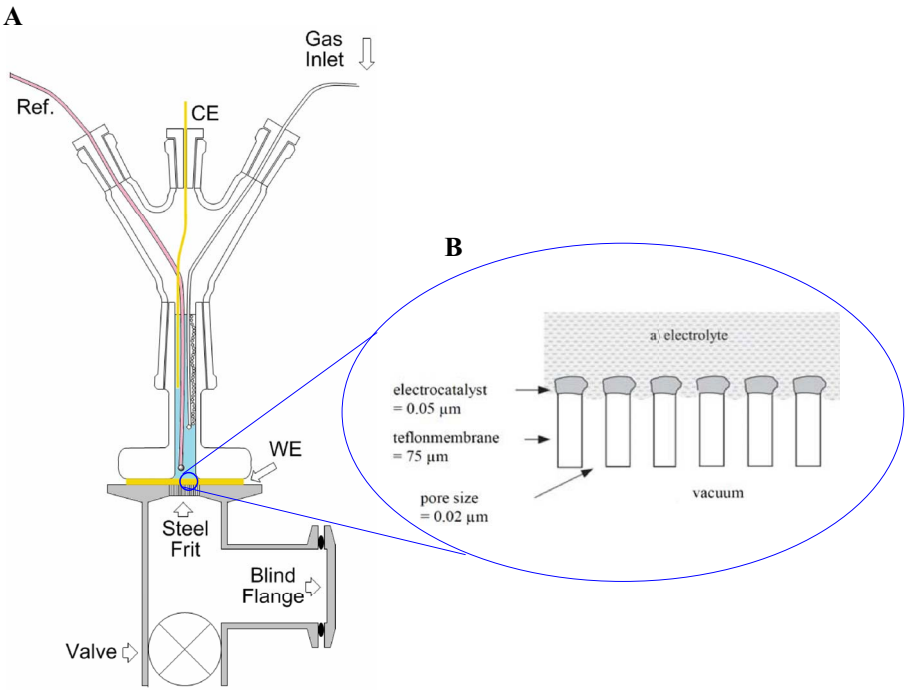

Figure 1. Conventional DEMS setup used in gas diffusion electrode experiments (A). A model of the gas diffusion working electrode (sputtered Teflon membrane) (B).

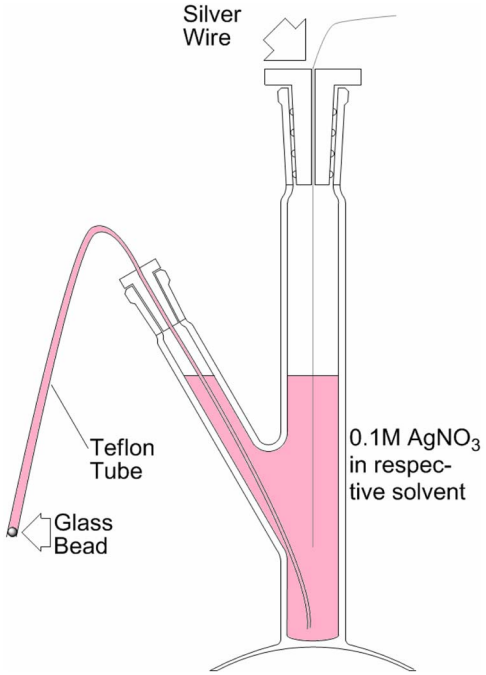

Figure 2. Design of the used Ag^+/Ag reference electrode: A silver wire is immersed in 0.1 M $AgNO_3$ solution. The solvent is either DMSO or NMP. A Teflon tube filled with silver solution and closed with a glass bead (with a roughened surface) ensures ionic contact to the electrolyte in the cell.

Highly pure lithium perchlorate ($LiClO_4$) (Sigma-Aldrich, $\geq 98\%$) used for preparing the electrolyte was dried under reduced pressure at 180°C until the weight was constant. $AgNO_3$ (AppliChem, *p. a grade*.) was used as received. *N*-methyl-2-pyrrolidone (NMP) (Sigma-Aldrich, anhydrous 99.5%) was used as received and extra dry dimethyl sulfoxide (DMSO) (Acros Organics, 99.7%) was dried in addition over activated molecular sieves. The water contents of the dried electolytes were checked using the Karl-Fischer titration method. Highly pure Ar (Air Liquid, 99.999%) was used for purging the electrolyte and highly pure oxygen (Air Liquid, 99.9995%) as a source for oxygen.

The Au-sputtered electrode was used as a gas diffusion electrode in some experiments. In contrast to the normal cell setup in which the electrolyte was saturated with oxygen, in these air was introduced from the gas side (the volume underneath the working electrode). Therefore, during the first cathodic going sweep, the valve (c.f. Figure 1) which directly connects the electrochemical cell to the vacuum system was closed and ion currents cannot be recorded. By removing the blind flange, atmospheric oxygen diffuses through the steel frit to the membrane where it is reduced at the electrode surface.

As soon as a potential of −1.25 V was reached, the potential sweep was stopped and the blind flange was mounted again. The volume underneath the electrode was then evacuated. By opening the valve, the electrochemical cell was directly connected to the mass spectrometer. In the first anodic sweep, the reduced oxygen species present at the electrode surface were oxidized and the ionic current of oxygen for mass 32 was recorded.

The calibration constant of DEMS (K°) is defined as the proportionality constant between the rate of species entering the mass spectrometer (dn_i/dt) and the corresponding ionic current I_i (eq 1):

$$I_i = K^o \left(\frac{dn_i}{dt}\right) = K^o \cdot \dot{n} \qquad [1]$$

The calibration leak experiment was performed under the same condition as the experiments.

The calibration leak was connected through a gas dosing valve to the T-piece which was directly connected with the cell and the vacuum system. The calibration volume of 54 mL was repeatedly evacuated with a Dual-stage rotary vane pump (DUO 2.5, Pfeiffer Vacuum) to ca. 0.02 mbar and purged with oxygen. A certain amount of calibrating gas (oxygen) was introduced into the volume to about 8 mbar. Once the dosing valve was opened to introduce the calibrating gas to the mass spectrometer with a defined flow rate, the reduction in the pressure was recorded via the attached gauge and the ionic current for mass 32 was recorded simultaneously.

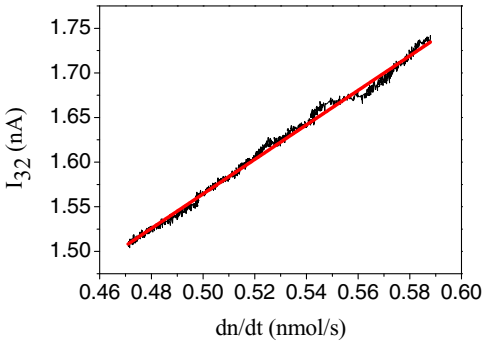

Figure 3. The linear relationship between the ionic current for mass 32 and the rate of oxygen molecules entering the mass spectrometer from calibration leak volume.

The linear relationship between the ionic current (I_i) vs. dn_i/dt gives a slope equal to the value of K° for a given gas as shown in Fig. 3.

Since the collection efficiency of the DEMS cell in use, the measured ion current and the calibration constant are all linked to some uncertainties.[35] It is therefore common practice to assume an error of ±10 to ±20% on DEMS results.[36–40] While we have found a high accuracy for the collection efficiency (ratio of formed species to those entering the vacuum system) of our cell in the past (close to 100% for this kind of cell), the calibration process comes along with uncertainties especially due to the pressure measurements - a well known problem in vacuum technology.

Results and Discussion

To demonstrate the suitability of the membrane we first performed typical DEMS experiments with the volume underneath the gas diffusion electrode being evacuated and connected to the MS in an electrolyte of 0.1 M Bu_4NClO_4 in NMP (Fig. 4A) and DMSO (Fig. 4B). The resulting curves are shown in Figure 4 and match well those curves shown in literature. Since the electrolyte is constantly purged with oxygen, there is a steady flow of molecules into the vacuum resulting in a relatively high baseline for mass 32, which was subtracted from the MSCV data shown in Fig. 4.

The potential was cathodically swept starting at –0.5 V. Oxygen was reduced at a potential of –1.22 V in NMP and of –1.05 V in DMSO and is re-evolved in the following anodic sweep at a potential of –1.38 V in NMP and at –1.15 V in DMSO, as seen in both the faradaic and ionic current. Obviously ORR and OER are the dominant reactions in DMSO. DEMS also allows for a quantitative correlation. This is not only true for O_2 evolution; at this type of electrode, the gas evolved is nearly quantitatively diffusing through the membrane into the vacuum of the MS. It is also true for oxygen reduction, where O_2 is consumed: the flow of oxygen into the vacuum is diffusion limited and according to Fick's law determined by the concentration gradient over the Nernstian diffusion layer. As the dimensions of the diffusion layer as well as the concentration gradient are fixed for a given experimental setup (i.e. a given convection as determined by the oxygen flow through the tubing), the overall flow of oxygen to the electrode and membrane $\frac{\partial n(O_2)}{\partial t} = \dot{n}_{tot}$ also is constant. As soon as the electrode approaches the potential of oxygen reduction a portion $\dot{n}_{el}$ of the influx is consumed electrochemically. Hence the flux of oxygen

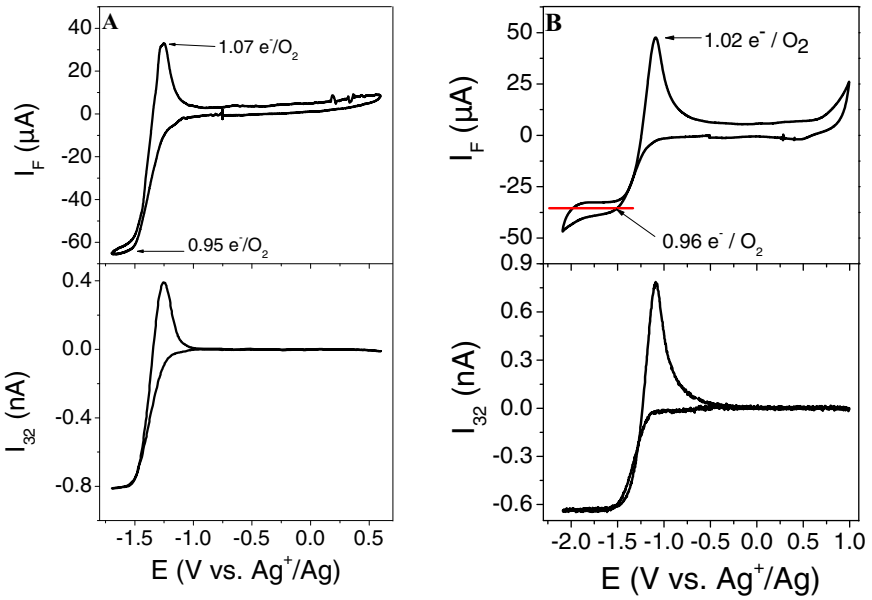

Figure 4. Simultaneously recorded CVs and MSCVs for mass 32 for oxygen reduction and evolution reactions at Au sputtered Teflon membrane in O_2-saturated electrolyte. 0.1 M $TBAClO_4$-NMP (A) and (B) 0.1 M $TBAClO_4$-DMSO based electrolytes. Scan rate: 10 mV/s.

entering the mass spectrometer $\dot{n}_{MS}$ is

$$\dot{n}_{MS} = \dot{n}_{tot} - \dot{n}_{el} \quad [2]$$

and thus

$$-I_I = K^0 \cdot \dot{n}_{el} + const \quad [3]$$

(In reality some O_2 originating from leaks and residual gas in the vacuum adds to this, resulting in a slowly changing baseline. Therefore, in the following, the baseline of ionic current is corrected.)

Since both, faradaic and ionic currents, are proportional to the amount of oxygen consumed and re-evolved, respectively, we can calculate from equation 4 the number of electrons transferred per molecule of oxygen (z in e^-/O_2) both upon reduction and evolution.

$$z = \frac{I_F \cdot K^\circ}{I_I \cdot F} \quad [4]$$

whereas I_F is the faradaic current with $I_F = zF\dot{n}_{el}$ assuming a current efficiency of 100%, I_I the ionic current, F the Faraday constant and K° a calibration constant determined in a calibration leak experiment as presented in details in the experimental section.

For DMSO we find 1.02 electrons upon oxygen reduction and 0.96 upon oxygen evolution. A value of z = 1 during oxygen reduction is indicative for the formation of superoxide. Therefore the formation of other reduced oxygen species such as peroxides is ruled out. Since the z-values observed during oxygen reduction and oxygen evolution match each other, side reactions are unlikely to occur. Side reactions are improbable to alter z-values for oxygen reduction and oxygen evolution in the same way. Therefore we can show here that oxygen is reduced to superoxide in an electrolyte of 0.1 M Bu_4NClO_4 in DMSO, thus supporting Loire et al. who came to this conclusion by purely kinetic considerations.[16]

The diffusion limited reduction current observed in Figure 4 was caused by the continuous bubbling with oxygen. Since the corresponding convection is not very strong, one might expect the typical diffusion limited peak as in cyclic voltammetry similar to the re-oxidation peak. Such a peak is not observed here because the transport of oxygen to the electrode is always diffusion limited: If oxygen is not consumed electrochemically it evaporates in to the vacuum. Since the product of reduction ($O_2^{-\bullet}$) is largely transported into the bulk of the electrolyte, only a small portion re-oxidized is to O_2.

In the case of NMP 0.95 e^-/O_2 are transferred during oxygen reduction and 1.07 e^-/O_2 are transferred during oxygen evolution. As in the case of DMSO superoxide is formed during oxygen reduction in a NMP-$TBAClO_4$ based electrolyte.

It is important to show that oxygen reduction both in DMSO and NMP based electrolytes results in superoxide formation when only TBA cations are present. This reaction can be used in future experiments to calibrate other DEMS cells such as flow trough cells and dual-thin-layer cells, where calibration through a leak is not an option.[41]

The results of a measurement performed in an electrolyte of 0.1 M $LiClO_4$ in DMSO are shown in Figure 5. The onset of oxygen reduction at −1.05 V is at the same potential as in the electrolyte containing 0.1 M Bu_4NClO_4. Oxygen evolution is shifted by 0.4 V to more positive potentials with respect to 0.1 M Bu_4NClO_4 containing electrolyte. Oxygen evolution in Figure 5 has an onset of −0.73 V and a peak potential of about –0.5 V. It is noteworthy that the electrode is completely deactivated at –1.75 V. During a full cathodic sweep 19.1 nmol of oxygen are reduced. If this oxygen is transformed into lithium

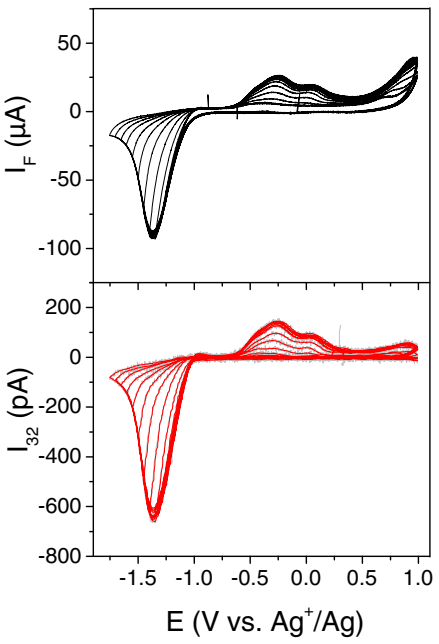

Figure 5. Simultaneously recorded CV (A) and MSCV for mass 32 (B) for oxygen reduction and evolution reactions at Au sputtered Teflon membrane in 0.1 M $LiClO_4$-DMSO based electrolyte. Scan rate: 20 mV/s.

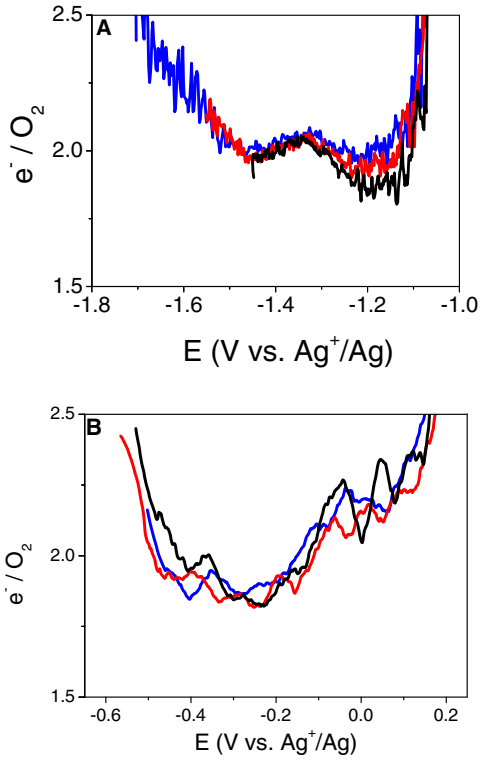

Figure 6. The calculated number of electrons transferred per oxygen molecule during the oxygen reduction (A) and (B) evolution reactions at Au sputtered Teflon membrane electrode in 0.1 M $LiClO_4$ in DMSO (A: cathodic sweep only). Scan rate: 20 mV/s. Lower potential limits are: Black: −1.45 V; Red: −1,55 V; Blue 1.70 V.

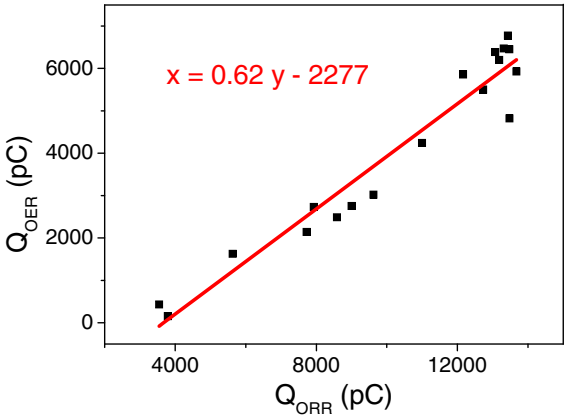

Figure 7. Ionic charge of oxygen evolution versus the ionic charge of oxygen reduction. The values are derived from each cycle shown in Figure 5.

peroxide this would correspond to the formation of just 3 monolayer (we define a monolayer as the ratio of Li_2O_2 units per surface atom of gold) of lithium peroxide - a very small amount to deactivate the electrode considering that Li_2O_2 is expected to form crystallites rather than a film.

Form equation 4, z was calculated for some cathodic sweeps shown in Figure 5. Calculations were done after correction for double layer capacity and the results are plotted in Figure 6, showing that roughly two electrons are transferred per molecule of oxygen. The increase in the number of electrons transferred as a potential of −1.6 V is passed is due to a side reaction that also occurs in Argon saturated electrolyte. In a potential range from −1.1 V to −1.6 V z roughly equals 2.

For the corresponding anodic sweeps of Figure 5, z-values have been calculated and are displayed in Figure 6B. The z-value at −0.25 V (where a peak is present in Figure 5) for oxygen evolution is about 1.9. This value fits well to the oxidation of peroxide. As the potential is increased further the z-value increases slightly to 2.2. This increase corresponds to the shoulder observed in Figure 5. At this point we have no explanation why oxygen evolution in the potential range from −0.67 V to 0.32 V proceeds in two distinct processes associated with a slight change in the electron number. But we note that the CVs in DMSO-based electrolyte at a gold electrode shown by Sharon et. al.,[42] by Laoire et al.,[16] by Peng et al.[12] and by us, differ from each other in the exact shape in the region of oxygen evolution. However the general features are the same in all cases. A peak during oxygen reduction is observed and oxygen evolution has an onset potential 300 mV more positive than the onset potential of oxygen reduction. In anodic direction there is a continuous current up to at least 0.1 V (4.0 V vs. Li^+/Li).

Literature findings that lithium peroxide is formed in organic electrolytes if Li^+ is present are based in their vast majority on *post mortem* analysis of discharged electrodes. However, this does not demonstrate that the amount of formed peroxide matches the charge transferred; the fact that lithium peroxide is the only product found does not mean that lithium peroxide is the sole reduction product, since discharge products might either not be accessible by the techniques employed or might remain in the electrolyte. McCloskey et al.[43] have already shown by means of DEMS that oxygen reduction in DMSO proceeds via the consumption of 2 electrons per molecule of oxygen. However this z-value was determined in a galvanostatic experiment, where the potential was around 2.7 V vs. Li^+/Li (−1.14 V vs. Ag^+/Ag) with a highly porous electrode. Peng et al. on the other hand reported a z-value ranging from 1.99 to 2.03 in a potentiostatic experiment but did not give any potential at which they determined those values. In fact a graphic evaluation of their curves results in an appreciable decrease of the z-value from roughly 2 to roughly 1 as the potential is decreased. The finding that oxygen reduction proceeds by the transfer of 2 electrons per molecule of oxygen in a potential window ranging from −1.1 V to −1.6 V at a rough electrode is of importance because it shows that no Li_2O is formed at potentials 400 mV lower than those used by McCloskey et al. at a rough gold electrode. Furthermore we are going to show in a subsequent paper that the z vs. E-plot differs from that shown in Figure 6 if a smooth gold electrode is used. (We would like to point out that a z-value of 2 for oxygen reduction would also be obtained, if the peroxide reacts with the solvent molecules in a subsequent reaction.)

The fact that oxygen reduction sets in at the same potential as in the electrolyte containing 0.1 M Bu_4NClO_4, despite the observation of lithium peroxide formation, might be taken as an indication that the first electron transfer is the rate determining step.

The true coulombic efficiency of the oxygen reduction/evolution is evaluated from the integrated ion currents during reduction and oxidation. In Fig. 5 the amount of reduced oxygen is altered by successively decreasing the lower potential limit. In Figure 7 the ionic charge of oxygen evolution of each cycle is plotted against the ionic charge of oxygen reduction of the respective cycle. The slope of the linear fit represents the true coulombic efficiency of the OER/ORR which is found here to be about 60%. It is interesting to note that the linear fit has a negative intercept with the y-axis. While a slope smaller than 1 means that in each cathodic sweep a certain percentage of the reduced oxygen is not re-oxidized in the following anodic sweep; a negative intercept means that a certain amount of the reduced oxygen is lost in each cycle. We are going to address this observation in a subsequent paper.

It is obvious, that this is not sufficient for a properly working lithium-air battery. On the other hand, Peng et al., have recently constructed a lithium-air battery and claim that it works on the basis of highly reversible formation and decomposition of lithium peroxide.[12] Peng et al. undertook much effort to show that the sole reaction product upon discharge is lithium peroxide using various spectroscopic methods. They show DEMS results (obtained with a swagelock type

Table I. Amounts of oxygen consumed and evolved from a lithium-air battery derived from the curves published by Peng et al.[12] From those values the true coulombic efficiency of OER/ORR was calculated.

Cycle number	$n(O_2)_{ORR}$ (mmol)	$n(O_2)_{OER}$ (mmol)	True coulombic efficiency (%)
1	0.39	0.18	46.11
5	0.30	0.13	43.69
10	0.33	0.15	45.67
100	0.26	0.19	72.90

cell) to confirm that only oxygen, but no CO_2, SO_2 or SO_3, is evolved during the anodic scan and that 2 electrons are transferred indeed both in the anodic and cathodic scan (*vide supra*).

However, they did not compare the amount of O_2 consumed with that evolved in the subsequent anodic cycle. We therefore calculated the true coulombic efficiency by integrating their curves, thus obtaining the amounts of reduced and evolved oxygen. The results are listed in Table I, with typical values below 50%. Therefore our results at model electrodes are in agreement with those of Peng et al. (but not with their interpretation) and confirm the results of McCloskey et al.,[4] which have found so far, undeservedly, little attention in literature among experimenters. With such a poor true coulombic efficiency the high cycling performance claimed by Peng et al. is bound to be due to some kind of side reaction. However, Peng et al. rule out the major formation of side products, based on several techniques (FTIR-, SERS-, ^{1}H–NMR and ^{13}C–NMR-spectroscopy). But the low sensitivity of NMR-spectroscopy is well known. In fact the ^{13}C-NMR-spectrum shown by Peng et al. features no signal from the carbon atoms of the conducting salt LiTFSI, which have fair intensity at a chemical shift of 120 ppm,[44,45] rendering the shown spectra meaningless. Furthermore different by-products other than the observed small amounts of HCO_2Li and Li_2CO_3 might form, undetectable by FTIR and SERS-spectroscopy. Therefore the high apparent cycleability of the lithium-air battery published by Peng et al. probably stems from the involvement of side reactions and the consumption of the electrolyte.

For instance, Sharon et al. have proposed a decomposition mechanism of DMSO resulting either in the formation of sulfate or of dimethylsolfone initiated by the deprotonation of one methyl group by either lithium hydroxide or superoxide and a subsequent nucleophilic attack at sulfur.[42] Such a mechanism might serve as an explanation for the reduced reversibility of oxygen reduction/evolution reactions. However other explanations are possible for the reduced reversibility of oxygen reduction/evolution reactions. For instance some of the formed peroxide might precipitate somewhere without electrical contact to the electrode or some larger particles might loss contact to the electrode in the course of oxygen evolution.

As mentioned above the gold sputtered Teflon membrane can also serve as a gas diffusion electrode. An experiment in which the electrode was used in such a way is shown in Figure 8. During the first cathodic sweep in 0.1M $LiClO_4$-DMSO based electrolyte, the electrode was exposed to laboratory air by closing the valve and opening the blind flange, thus filling the volume underneath the electrode with air which has been evacuated previously. During the first cathodic sweep there was no oxygen reduction until the current begins to decrease at a potential of −0.72 V. As soon as a potential of −1.25 V is reached the potential was stopped and the blind flange was mounted again. The volume underneath the electrode then was evacuated by opening the valve, thus connecting the electrochemical cell to the mass spectrometer. As the supply of oxygen from underneath the electrode is cut-off the current drops to zero.

Since there was no connection to the mass spectrometer no ionic current was recorded during the first cathodic sweep; nevertheless in the following anodic sweep the oxidation of those oxygen species

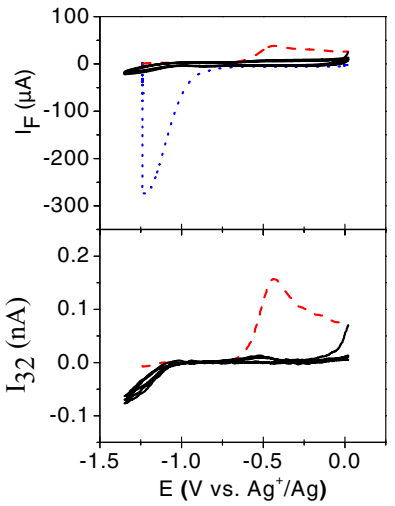

Figure 8. Simultaneously recorded CV (a) and MSCV for mass 32 (b) during oxygen reduction and evolution reactions at gas diffusion electrode (Au sputtered Teflon membrane) in 0.1 M $LiClO_4$-DMSO based electrolyte. Oxygen source is atmospheric air in the first cathodic going sweep, electrolyte purged with oxygen. Blue: first cathodic going sweep; red: first anodic going sweep; Black: ensuing cycles with oxygen supplied from solution. Sweep rate 10 mV/s.

formed in the first cathodic sweep were observed by mass spectroscopy.

In the subsequent cycles, the dissolved oxygen in the electrolyte was reduced. It is obvious that much larger current are obtained when the electrode is employed as a gas diffusion electrode, since oxygen transport is much more efficient from gas phase then by diffusion through a liquid.

It is important to show that also under these ambient conditions oxygen reduction and evolution takes place as well. This can be seen from the ionic current in the first anodic sweep. But a major drawback is the lower true coulombic efficiency of OER/ORR under these conditions, amounting only to 16% (derived from faradaic current). The reason for that may be humidity and also CO_2. In the presence of CO_2, carbonate is formed as has been shown previously by both theoretical calculations and post mortem analysis.[46]

Similar to the gas diffusion experiment shown in Figure 8, the CVs and in situ MSCVs for ORR and OER in 0.1 M $LiClO_4$-NMP based electrolyte containing 60 and 380 ppm of water were recorded starting at −0.2 V vs. $Ag^+/Ag_{(NMP)}$ as shown in Figure 9A and 9B respectively. That figure shows the sweep starting at −0.2 V in the negative going scan where the GDE was exposed to the atmospheric air from the gas side. In the beginning of the cathodic sweep, the current is close to zero because no oxygen reduction reaction takes place. The onset potential for ORR is −0.86 V whereas the faradaic current starts to decrease followed by the reduction peak of oxygen at −1.35 V with a current density of 500 $\mu A/cm^2$ (based on geometric surface area). The sweep was held once the potential reached −1.35 V. The electrochemical cell was then directly connected to the mass spectrometer by opening the valve (Figure 1) after evacuating the volume underneath the electrode.

In the following anodic going sweep the evolution of oxygen was observed in the MSCV. Oxygen evolution has an onset potential of −0.69 V and continues to proceed until the upper potential limit is reached with peaks at −0.46 V and 0.52 V respectively. Major amounts of oxygen are evolved at potentials more positive than 0.23 V paralleled by the evolution of a signal for mass 44 after the electrode was employed as a GDE electrode. In the following cycles in which oxygen is reduced from solution, most of the oxygen is evolved in a potential range from −0.7 to 0.0 V, while the signal intensity for mass 44 is reduced. Although NMP causes a high baseline for mass 44 due to a fragment formed during the ionization process, there is no reason why this baseline should be dependent on the potential applied to the

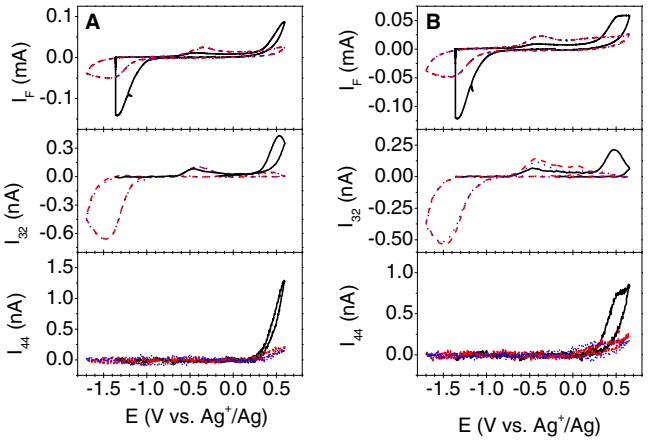

Figure 9. Simultaneously recorded CV and MSCVs for mass 32 and mass 44 during oxygen reduction and evolution at gas diffusion electrode (Au sputtered Teflon membrane) in 0.1 M $LiClO_4$-NMP based electrolyte containing (A) 60 and (B) 380 ppm of water. Oxygen source is atmospheric air in the first cathodic going sweep, electrolyte purged with oxygen. Sweep rate 10 mV/s. Black: 1st cycle, electrode was used as a GDE; Red and blue: 2nd and 3rd cycle, oxygen was supplied from solution.

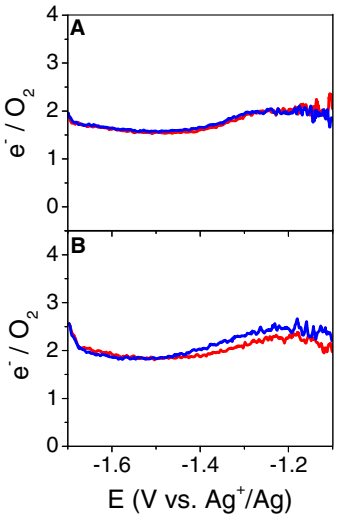

Figure 11. z-value of ORR as a function of potential in a NMP-$LiClO_4$ based electrolyte. The z-value has been calculated for the curves shown in Figure 9. A: Water content: 60 ppm, B: water content: 380 ppm. Colors are as indicated in Figure 9.

electrode. Hence the evolution of a signal for mass 44 is probably due to the formation of CO_2. But the only source of carbon in the system under investigation is NMP. Hence the evolution of CO_2 indicates the decomposition of the electrolyte.

Since there is no CO_2 evolution observable in the same potential range when the electrode is cycled in Ar-saturated electrolyte (c.f. Figure 10) and as with decreasing amounts of reduced oxygen in the previous cathodic sweeps there are also decreasing amounts of CO_2 evolved, there is clearly a connection between oxygen reduction and CO_2 evolution. As with DMSO, oxygen reduction proceeds via the transfer of 2 electrons per molecule of oxygen (c.f. Figure 11). Hence also here oxygen is reduced to peroxide. But as pointed out in the case of DMSO the formation of peroxide does not mean that it precipitates as lithium peroxide. In the case of NMP at least parts of the formed peroxide react with the electrolyte to form some compound that ultimately reacts to form CO_2 in the next anodic cycle at potentials above 0.1 V.

The black curves in Figure 12 show that the z-value in this potential region is 2 when the electrode was used as a gas diffusion electrode in the previous cathodic sweep. However in the same potential range 3 to 7 e^-/O_2 were transferred when oxygen was supplied to the electrode from solution. While a z-value of 2 fits nicely with the oxidation of peroxide a value of 3 or even 7 is much to large to assume oxygen evolution as the only source of faradaic current.

In Figure 12C the anodic sweeps of the CV already displayed in Figure 9A are shown in more detail. In the black curve the peak potential is at −0.46 V. But at this potential only a faint shoulder appears in the red and blue curves while the peak potential shifts by 120 mV to a less negative potential of –0.34 V. The corresponding

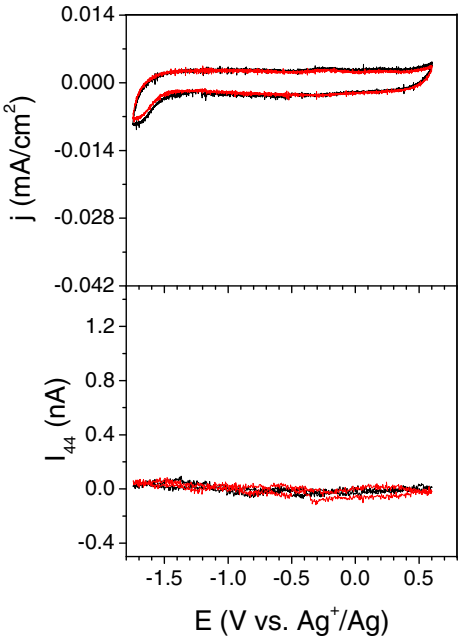

Figure 10. Simultaneously recorded CV and MSCV for mass 44 in Ar-saturated 0.1 M $LiClO_4$-NMP based electrolyte.

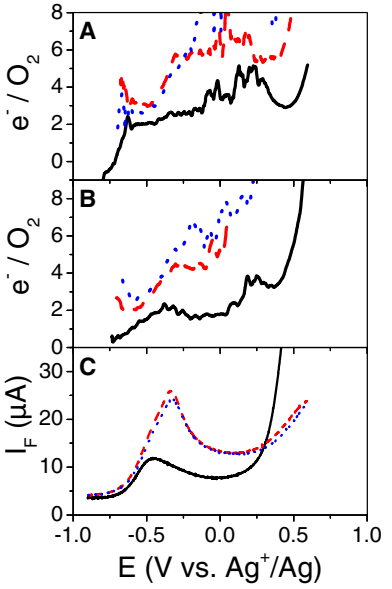

Figure 12. z-value of OER as a function of potential in a NMP-$LiClO_4$ based electrolyte. The z-value has been calculated for the curves shown in Figure 9. A: Water content: 60 ppm, B: water content: 380 ppm. C: expended faradaic current of Figure 9. Colors are as indicated in Figure 9.

shift of the peak potential in the MSCV for mass 32 is only 30 mV. Hence some other reaction appears in the anodic sweep unrelated to the OER when oxygen was reduced from solution in the previous cathodic sweep. This reaction is superimposed to peroxide oxidation and increases therefore the observed z-value significantly.

As pointed out already in the introduction there should not be any effect like pore clogging or diffusion effects in pores with the electrode employed in this experiment. Therefore whether the electrode is supplied with oxygen from solution or from the gas phase should not have any effect on the shape of the CV other than the observed current densities. However in those experiments where oxygen is reduced from the solution side, smaller quantities of peroxide are formed. If a stepwise degradation process of NMP is assumed then a lower concentration of peroxide might lead to the formation of other decomposition products than would be observed with larger peroxide concentrations. Large peroxide concentrations in NMP would then lead to decomposition products that are oxidized at potentials higher than 0.1 V to form CO_2, while lower peroxide concentrations lead to decomposition products that are electrooxidized at –0.34 V close to the potential of peroxide oxidation.

The evolution of oxygen in the second peak might be due to the oxidation of organic peroxides, but might also stem from lithium peroxide embedded and insulated from the electrode by a matrix of decomposition products. As this matrix is oxidized and removed from the electrode, the lithium peroxide regains electrical contact to the electrode and is oxidized as well. Despite the presence of lithium peroxide in the later case, electrocatalysis of electrolyte oxidation is improbable as CO_2-evolution causes lithium peroxide to regain contact with the electrode, rather than lithium peroxide in contact with the electrode causes CO_2-evolution.

Decomposition of NMP upon oxygen reduction has previously been found by Wang et al.[14] The mechanism the authors give is based on the abstraction of protons by superoxide and a subsequent oxidation both electrochemically and chemically by oxygen. However as we find no evidence for electrolyte decomposition upon oxygen reduction in NMP-TBAClO_4 based electrolyte this mechanism probably is not correct.

McCloskey et al. who have observed CO_2 evolution in NMP based electrolyte also used an electrode made of carbon for their experiments.[29] Therefore their assignment of CO_2-evolution to electrolyte oxidation is not beyond doubt, as the carbon-electrode is another probable source of CO_2 evolution. Furthermore McCloskey at el. suggested the electrooxidation of the electrolyte to be due to the defect states in the semiconductor Li_2O_2 resulting in an electrocatalytic effect. But in Figure 9A oxygen evolution from Li_2O_2 in contact with Au terminates before a potential of 0.1 V is reached. Hence no lithium peroxide with electronic contact to the electrode is left and no electrocatalytic effect due to defective states in Li_2O_2 is possible.

Figures 9A and 9B do not differ from each other significantly in shape. However the ratio of evolved to reduced oxygen is seemingly more favorable in the case of the electrolyte containing 380 ppm water. In those cycles of Figure 9B where oxygen is reduced from solution the ratio was on average 29% while in the electrolyte with a water content of only 60 ppm the ratio was on average 18.5%. On the other hand, when the electrode is used as a GDE then nearly the same faradaic charge is transferred but in the electrolyte with water content of 380 ppm only half the amount of oxygen is evolved than in the experiment with a water content of 60 ppm. We cannot give any explanation for this contradicting behavior, but we note that the presence of water seems to have some influence on oxygen reduction in NMP. To some extend this is not surprising as 60 ppm and 380 ppm of water content correspond to a water concentration of 3.4 and 21.7 mmol/l respectively. Both values are relatively high as compared to the solubility of oxygen in NMP, which is 3.2 mmol/l.[47] But on the other hand with a pk_a value of 31.2 of water on the Brodwell scale[48] and a virtually non-existing proton concentration the source of any effect of water is hard to imagine. A possible effect might result from the participation of water in the solvation sphere of the Li-ions.

Conclusions

The experiments show that under ambient conditions with humidity and in presence of CO_2, oxygen can be reduced from atmospheric air at a gold sputtered membrane used as a gas diffusion electrode. In this way we achieve very high current densities upon discharge of up to 0.53 mA/cm^2 in case of NMP and 0.97 mA/cm^2 in case of DMSO. However, the true coulombic efficiency of OER/ORR (as obtained from mass spectrometric ion currents) differs clearly from 100% and side reactions take place in both NMP and DMSO based electrolytes. Therefore, a cycleable and highly reversible secondary lithium-air battery with a DMSO based electrolyte is unlikely to work purely on the principle of reversible formation of lithium peroxide.

By employing in situ techniques we were able to confirm that in presence of Li^+-ions oxygen reduction results in the formation of peroxide in both DMSO and NMP. For DMSO it has been shown that 2 electrons per molecule of oxygen are transferred ranging from –1.1 to –1.6 V. No indications for the formation of Li_2O have been found.

We have found that superoxide is formed upon oxygen reduction in TBA containing electrolyte. This claim has previously been based only on kinetic considerations. The importance of this finding is that this reaction can be used in future studies to calibrate DEMS cells, where leakage calibration is not an option and a known reproducible electrochemical reaction is required.

It has been shown that NMP decomposes during the reduction of oxygen in the presence of Li^+. The decomposition is probably induced by peroxide and results in different decomposition products depending on the concentration of formed peroxide.

Acknowledgment

The authors acknowledge the Federal Ministry of Education and Research for funding this work. This work is part of the “LuLi – Strom aus Luft und Li” project (FKZ:03X4624A).

References

1. K. M. Abraham and Z. Jiang, *Journal of the Electrochemical Society*, **143**, 1 (1996).
2. P. G. Bruce, S. A. Freunberger, L. J. Hardwick, and J.-M. Tarascon, *Nature Materials*, **11**, 19 (2012).
3. S. R. Gowda, A. Brunet, G. M. Wallraff, and B. D. McCloskey, *The Journal of Physical Chemistry Letters*, **4**, 276 (2013).
4. B. D. McCloskey, D. S. Bethune, R. M. Shelby, G. Girishkumar, and A. C. Luntz, *The Journal of Physical Chemistry Letters*, **2**, 1161 (2011).
5. F. Mizuno, S. Nakanishi, Y. Kotani, S. Yokoishi, and H. Iba, *Electrochemistry*, **78**, 403 (2010).
6. K. Xu, *Chemical Reviews*, **104**, 4303 (2004).
7. H. Kim, G. Jeong, Y.-U. Kim, J.-H. Kim, C.-M. Park, and H.-J. Sohn, *Chemical Society Reviews*, **42**, 9011 (2013).
8. J. Read, *Journal of the Electrochemical Society*, **153**, A96 (2006).
9. H.-G. Jung, J. Hassoun, J.-B. Park, Y.-K. Sun, and B. Scrosati, *Nature Chemistry*, **4**, 579 (2012).
10. S. A. Freunberger, Y. Chen, N. E. Drewett, L. J. Hardwick, F. Barde, and P. G. Bruce, *Angewandte Chemie-International Edition*, **50**, 8609 (2011).
11. C. O. Laoire, S. Mukerjee, E. J. Plichta, M. A. Hendrickson, and K. M. Abraham, *Journal of the Electrochemical Society*, **158**, A302 (2011).
12. Z. Peng, S. A. Freunberger, Y. Chen, and P. G. Bruce, *Science*, **337**, 563 (2012).
13. M. J. Trahan, S. Mukerjee, E. J. Plichta, M. A. Hendrickson, and K. M. Abraham, *Journal of the Electrochemical Society*, **160**, A259 (2013).
14. H. Wang, K. Xie, L. Wang, and Y. Han, *Journal of Power Sources*, **219**, 263 (2012).
15. V. S. Bryantsev, V. Giordani, W. Walker, M. Blanco, S. Zecevic, K. Sasaki, J. Uddin, D. Addison, and G. V. Chase, *Journal of Physical Chemistry A*, **115**, 12399 (2011).
16. C. O. Laoire, S. Mukerjee, K. M. Abraham, E. J. Plichta, and M. A. Hendrickson, *Journal of Physical Chemistry C*, **114**, 9178 (2010).
17. W. Xu, J. Hu, M. H. Engelhard, S. A. Towne, J. S. Hardy, J. Xiao, J. Feng, M. Y. Hu, J. Zhang, F. Ding, M. E. Gross, and J.-G. Zhang, *Journal of Power Sources*, **215**, 240 (2012).
18. D. Xu, Z.-l. Wang, J.-j. Xu, L.-l. Zhang, L.-m. Wang, and X.-b. Zhang, *Chemical Communications*, **48**, 11674 (2012).
19. M. M. Ottakam Thotiyl, S. A. Freunberger, Z. Peng, Y. Chen, Z. Liu, and P. G. Bruce, *Nature Materials*, **12**, 1050 (2013).
20. A. A. Abd-El-Latif and H. Baltruschat, in *Encyclopedia of Applied Electrochemistry*, G. Kreysa, K.-i. Ota and R. Savinell Editors, p. 507 Springer New York Dordrecht Heidelberg London (2014).
21. G. Eggert and J. Heitbaum, *Electrochimica Acta*, **31**, 1443 (1986).

22. R. Imhof and P. Novak, *Journal of the Electrochemical Society*, **145**, 1081 (1998).
23. R. Imhof and P. Novak, *Journal of the Electrochemical Society*, **146**, 1702 (1999).
24. P. Novak, J. C. Panitz, F. Joho, M. Lanz, R. Imhof, and M. Coluccia, *Journal of Power Sources*, **90**, 52 (2000).
25. M. Hahn, A. Wursig, R. Gallay, P. Novak, and R. Kotz, *Electrochem. Commun.*, **7**, 925 (2005).
26. P. Novak, D. Goers, L. Hardwick, M. Holzapfel, W. Scheifele, J. Ufhiel, and A. Wursig, *Journal of Power Sources*, **146**, 15 (2005).
27. J. Ufheil, A. Wursig, O. D. Schneider, and P. Novak, *Electrochemistry Communications*, **7**, 1380 (2005).
28. T. Ogasawara, A. Débart, M. Holzapfel, P. Novák, and P. G. Bruce, *Journal of the American Chemical Society*, **128**, 1390 (2006).
29. B. D. McCloskey, D. S. Bethune, R. M. Shelby, T. Mori, R. Scheffler, A. Speidel, M. Sherwood, and A. C. Luntz, *The Journal of Physical Chemistry Letters*, **3**, 3043 (2012).
30. B. D. McCloskey, R. Scheffler, A. Speidel, G. Girishkumar, and A. C. Luntz, *Journal of Physical Chemistry C*, **116**, 23897 (2012).
31. C. J. Barile and A. A. Gewirth, *Journal of The Electrochemical Society*, **160**, A549 (2013).
32. N. Tsiouvaras, S. Meini, I. Buchberger, and H. A. Gasteiger, *Journal of the Electrochemical Society*, **160**, A471 (2013).
33. H. Baltruschat, in *Interfacial Electrochemistry*, A. Wieckowski Editor, p. 577 Marcel Dekker, Inc., New York, Basel (1999).
34. G. Gritzner, *Journal of Molecular Liquids*, **156**, 103.
35. S. J. Aston, Design, Construction and Research Application of a Differential Electrochemical Mass Spectrometer (DEMS), in *Department of Chemistry*, p. 224, University of Copenhagen, Copenhagen (2012).
36. R. Stadler, Z. Jusys, and H. Baltruschat, *Electrochimica Acta*, **47**, 4485 (2002).
37. T. Löffler, R. Bussar, E. Drbalkova, P. Janderka, and H. Baltruschat, *Electrochimica Acta*, **48**, 3829 (2003).
38. N. Fietkau, R. Bussar, and H. Baltruschat, *Electrochimica Acta*, **51**, 5626 (2006).
39. U. Müller and H. Baltruschat, *The Journal of Physical Chemistry B*, **104**, 5762 (2000).
40. T. Löffler, R. Bussar, X. Xiao, S. Ernst, and H. Baltruschat, *Journal of Electroanalytical Chemistry*, **629**, 1 (2009).
41. H. Baltruschat, *J. Am. Soc. Mass Spectrom.*, **15**, 1693 (2004).
42. D. Sharon, M. Afri, M. Noked, A. Garsuch, A. A. Frimer, and D. Aurbach, *The Journal of Physical Chemistry Letters*, **4**, 3115 (2013).
43. B. D. McCloskey, D. S. Bethune, R. M. Shelby, T. Mori, R. Scheffler, A. Speidel, M. Sherwood, and A. C. Luntz, *The Journal of Physical Chemistry Letters*, **3**, 3043.
44. I. Nicotera, C. Oliviero, W. A. Henderson, G. B. Appetecchi, and S. Passerini, *The Journal of Physical Chemistry B*, **109**, 22814 (2005).
45. R. Arvai, F. Toulgoat, B. R. Langlois, J.-Y. Sanchez, and M. Médebielle, *Tetrahedron*, **65**, 5361 (2009).
46. H.-K. Lim, H.-D. Lim, K.-Y. Park, D.-H. Seo, H. Gwon, J. Hong, W. A. Goddard, H. Kim, and K. Kang, *Journal of the American Chemical Society*, **135**, 9733 (2013).
47. J. Read, K. Mutolo, M. Ervin, W. Behl, J. Wolfenstine, A. Driedger, and D. Foster, *Journal of the Electrochemical Society*, **150**, A1351 (2003).
48. F. G. Bordwell, *Accounts of Chemical Research*, **21**, 456 (1988).